



HAL
open science

Personalization of Cardiac Motion and Contractility from Images using Variational Data Assimilation

Hervé Delingette, Florence Billet, Ken C.L. Wong, Maxime Sermesant, Kawal S. Rhode, Matt Ginks, C. Aldo Rinaldi, Reza Razavi, Nicholas Ayache

► **To cite this version:**

Hervé Delingette, Florence Billet, Ken C.L. Wong, Maxime Sermesant, Kawal S. Rhode, et al.. Personalization of Cardiac Motion and Contractility from Images using Variational Data Assimilation. IEEE Transactions on Biomedical Engineering, 2012, 59 (1), pp.20-24. 10.1109/TBME.2011.2160347 . inria-00616183

HAL Id: inria-00616183

<https://inria.hal.science/inria-00616183v1>

Submitted on 8 Jul 2013

HAL is a multi-disciplinary open access archive for the deposit and dissemination of scientific research documents, whether they are published or not. The documents may come from teaching and research institutions in France or abroad, or from public or private research centers.

L'archive ouverte pluridisciplinaire **HAL**, est destinée au dépôt et à la diffusion de documents scientifiques de niveau recherche, publiés ou non, émanant des établissements d'enseignement et de recherche français ou étrangers, des laboratoires publics ou privés.

Personalization of Cardiac Motion and Contractility from Images using Variational Data Assimilation

H. Delingette, F. Billet, K. C. L. Wong, M. Sermesant, K. Rhode, M. Ginks, C. A. Rinaldi, R. Razavi, N. Ayache

Abstract—Personalization is a key aspect of biophysical models in order to impact clinical practice. In this paper, we propose a personalization method of electromechanical models of the heart from cine MR images based on the adjoint method. After estimation of electrophysiological parameters, the cardiac motion is estimated based on a proactive electromechanical model. Then cardiac contractilities on two or three regions are estimated by minimizing the discrepancy between measured and simulation motion. Evaluation of the method on three patients with infarcted or dilated myocardium is provided.

Index Terms—Cardiac Modelling, Personalization

I. INTRODUCTION

The objective of biophysical cardiac modeling is to improve the understanding of the cardio-vascular system by performing numerical simulation of the cardiac function from its mathematical description. Simulations of the whole organ have reached such a degree of realism that it is now possible to compare them quantitatively with available cardiac images and signals acquired routinely on patients. This has led to a new vision and a potential impact of those models in the clinical practice: improving the diagnosis of cardiac diseases and planning therapies (such as Cardiac Resynchronization Therapy [1]) from personalized biophysical models. Model personalization consists in optimizing some parameters of the model such that it behaves in adequacy with patient specific datasets (images and signals). This personalization can be split into two separate stages: geometrical personalization and biophysical personalization (see Fig. 1).

In the former case, the computational mesh is built from patient-specific anatomical images based on medical image analysis algorithms. In the latter case, the parameters of the models, initial and boundary conditions are optimized such that cardiac simulations match observations from images. Solving this inverse problem is a complex task for the following reasons: i) it is very time consuming and convergence is not guaranteed; ii) the information extracted from images is usually very sparse spatially and temporally iii) only a subset of the parameters may be observed and thus estimated. Furthermore, parameter estimation of dynamic systems often leads to mathematically involved methods.

Several approaches for cardiac model personalization have been proposed with various parameters to be optimized and optimization methods. Moireau *et al.* [2] used reduced

H. Delingette, K. C. L. Wong, F. Billet, M. Sermesant and N. Ayache are with INRIA, Asclepios team, Sophia Antipolis, France

K. Rhode, M. Ginks, C. A. Rinaldi and R. Razavi are with King’s College London, Division of Imaging Sciences and Biomedical Engineering, St. Thomas’ Hospital, UK.

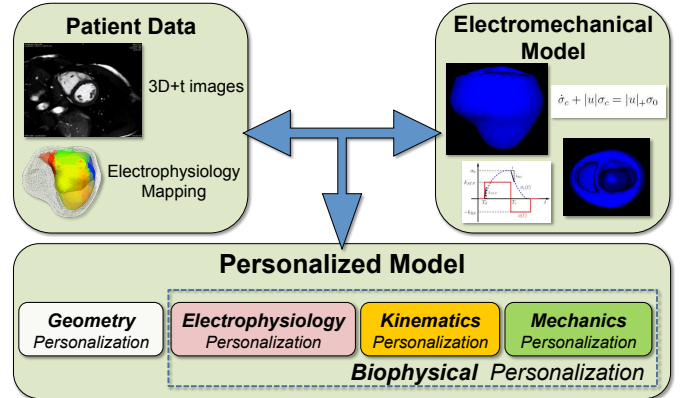


Fig. 1. Electromechanical Models Personalization from Images and Signals.

Unscented Kalman Filtering (rUKF) to estimate contractility parameters from synthetic image sequences. Xi *et al.* [3] compared rUKF and sequential Quadratic Programming (SQP) for the estimation of passive stiffness parameters on synthetic data. Wang *et al.* [4] estimated passive material stiffness with a SQP method from tagged MRI and ex vivo DT-MRI of canine hearts. Liu *et al.* [5] used extended Kalman Filtering to estimate passive stiffness parameters on 2D slices from tagged and cine MR canine images. In [6], Sundar *et al.* proposed an adjoint method to estimate contractility parameters from synthetic cardiac motion data.

In this article, we demonstrate a novel personalization method of a 3D cardiac model from catheterized electrophysiology data and cine MR images from three patients. The biophysical personalization is broken into three successive stages: *electrophysiology*, *kinematics* and *mechanical* personalization. A first contribution of our approach is to include an electromechanical model for the motion estimation stage (kinematics personalization) in order to produce a *regularized* motion. A second contribution is to propose an adjoint based method to estimate contractility parameters on the right ventricle (RV) and left ventricle (LV) as well as scar regions. Finally, we present a first automated method for biophysical personalization combining electrophysiology and mechanics.

II. ELECTROPHYSIOLOGY AND KINEMATICS PERSONALIZATION

A. Electrophysiology Personalization

In order to avoid accumulating sources of uncertainties, we are considering in this paper patient specific datasets that include a rich description of cardiac electrophysiology. More

precisely, in addition to the acquisition of anatomical and cine-MR images, non-contact endocardial mappings have been acquired at the St Thomas' Hospital during electrophysiology studies in an XMR suite [7] both in sinus rhythm and during specific stimulation protocols. The extracted depolarization and repolarization isochrones then serve as input information to an electrophysiology personalization method [8] which minimizes the discrepancy between measured and simulated isochrones. Its output is a set of global parameters and local parameters (electrical conductivities...) of the Mitchell-Schaeffer electrophysiology model which allow to interpolate, extrapolate and regularize the acquired isochrones. The personalized depolarization and repolarization times are then used to control the active contraction force of the mechanical model described in the next section.

B. Kinematics Personalization

Kinematics personalization consists in estimating the motion of cardiac structures from images. We use the same electromechanical model both to regularize the cardiac motion from cine-MR images and to estimate biophysical parameters. Indeed, this leads to an estimation of velocity fields which is consistent in terms of smoothness and spatial resolution with the ones produced by our electromechanical model used for the mechanical parameter estimation.

The kinematics personalization approach described in [9] is based on a proactive deformable model [10] including three mechanical components: transmembrane potential propagation, active contraction forces, and passive biomechanics. The two ventricles are meshed with tetrahedra from anatomical MR images. The evolution of the displacement \mathbf{U} of each mesh node is governed by the following equation:

$$\mathbf{M}\ddot{\mathbf{U}} + \mathbf{C}\dot{\mathbf{U}} + \mathbf{K}\mathbf{U} = \mathbf{F}_b + \mathbf{F}_c + \beta\mathbf{F}_{\text{img}} \quad (1)$$

where \mathbf{M} , \mathbf{C} , and \mathbf{K} are the mass, damping, and stiffness matrices respectively, \mathbf{F}_b is the external load from boundary conditions (blood pressure, valves), \mathbf{F}_c is the force vector for active contraction. This contraction force is applied along a local fiber orientation and is controlled by several parameters including the maximum contraction parameter σ_0 . Furthermore, spring boundary conditions [10] are applied to points located at the base of the ventricles.

In the kinematics personalization, we also add the term \mathbf{F}_{img} corresponding to a force vector which tracks salient image features in the image sequence. More precisely, \mathbf{F}_{img} is computed using a 3D block-matching algorithm to attract points towards the closest edge voxels. To balance between motion regularization and data attachment, we set the β parameters based on a sensitivity analysis [11]. Image forces are not physiology based since their sole purpose is to help tracking the cardiac motion. They are discarded during the mechanical personalization.

III. MECHANICAL PERSONALIZATION BASED ON VARIATIONAL DATA ASSIMILATION

A. Adjoint Method for Parameter Estimation

Parameter estimation of biophysical cardiac models is a fairly new problem receiving a growing interest. Sequential

and variational methods are among the most popular data assimilation techniques. Sequential methods such as rUKF have been proposed recently for the parameter estimation of contractility or passive stiffness parameters on synthetic data [2], [3]. While very promising, these methods do not handle well the phase changes of the cardiac cycle, which are an important aspect of the heart behavior. Also, preliminary work based on variational data assimilation (with [6] or without [12] solving the adjoint equation) have also been performed on synthetic data.

In this article, we use a variational data assimilation approach based on the adjoint model and evaluate it on three cine MRI cases. It is based on the minimization of a functional measuring the discrepancy between simulation and measurements, in our case the node positions previously estimated from the kinematics personalization using image forces:

$$\mathcal{F} = \sum_{n=0}^N \sum_{i \in V_n} \frac{1}{2} \| {}^i Y_M^n - {}^i Y_K^n \|^2$$

where N is the number of images in the image sequence, V_n is the set of nodes visible in images n , ${}^i Y_M^n$ (resp. ${}^i Y_K^n$) is the position of the node i at time n of the mechanically (resp. kinematically) personalized mesh.

Among the various parameters of the model, we choose to estimate contractility parameters $\Sigma_0 = \{\sigma_0^R, \sigma_0^L, \sigma_0^S\}$ of the right and left ventricles and eventually scar regions. Those parameters can be mostly observed during systole while passive stiffness parameters can be mostly observed during diastole. More precisely, to observe contractilities one would need to measure also the endocardial pressure in addition to cardiac motion. With only the latter, we can only estimate the ratio between contractilities and passive stiffnesses which can be considered as *apparent contractilities*.

The optimization of functional $\mathcal{F}(\Sigma_0)$ is performed using a quasi-Newton BFGS-B with bound constraint. This optimizer requires the computation of the functional gradient with respect to each contractility parameter σ_0 which is performed using the adjoint method. More precisely, the discretization of Equation 1 with finite elements (in space) and Houbolt integration scheme (in time) leads to a recurrence relation : $\mathbf{K}^{t+1}\mathbf{Y}_M^{t+1} = \mathbf{A}_0^t\mathbf{Y}_M^t + \mathbf{A}_1^t\mathbf{Y}_M^{t-1} + \mathbf{A}_2^t\mathbf{Y}_M^{t-2} + \mathbf{F}^t$ where \mathbf{Y}_M^t is the node position vector at time t , \mathbf{K}^t and $\{\mathbf{A}_i^t\}$ are stiffness matrices and \mathbf{F}^t is the force vector at time t . Therefore minimizing functional \mathcal{F} is equivalent to the minimization under constraint:

$$\mathcal{L}(\{\mathbf{Y}_M^t\}, \{\mathbf{P}^t\}, \Sigma_0) = \mathcal{F}(\{\mathbf{Y}_M^t\}, \Sigma_0) + \sum_{t=0}^{t_f} (\mathbf{P}^t)^T \left(\mathbf{K}^{t+1}\mathbf{Y}_M^{t+1} - \sum_{i=0}^2 \mathbf{A}_i^t \mathbf{Y}_M^{t-i} - \mathbf{F}^t \right)$$

where \mathbf{P}^t is the Lagrange multiplier associated with the recurrence relation at time t and t_f is the total number of iterations. In this functional, only the terms \mathbf{F}^t and eventually \mathbf{K}^t , \mathbf{A}^t depend on the contractility parameters Σ_0 . However, $\partial\mathcal{L}/\partial\Sigma_0$ also involves the Lagrange multiplier \mathbf{P}^t . By writing that $\partial\mathcal{L}/\partial\mathbf{Y}_M^t = 0, \forall t$, one obtains a recurrence equation only involving \mathbf{P}^j , \mathbf{Y}^j and \mathbf{A}_i^j $j \in [t-3, t+3]$ corresponding to the adjoint model.

In summary, to estimate $\partial\mathcal{L}/\partial\Sigma_0$, we first compute the Lagrange multipliers using the recurrence equation found by setting $\partial\mathcal{L}/\partial\mathbf{Y}^t = 0$. This recurrence is solved backward starting from $\mathbf{P}^{t_f} = 0$. We then compute $\partial\mathbf{A}_i^t/\partial\Sigma_0$ and $\partial\mathbf{F}^t/\partial\Sigma_0$ and finally obtain $\partial\mathcal{L}/\partial\Sigma_0$ using chain rule derivation.

In our electromechanical model, $\partial\mathbf{A}_i^t/\partial\Sigma_0 = 0$ and all stiffness matrices are constant. However, we have to deal with the isovolumetric contraction and relaxation phases which provide additional constraints. Also, we removed the Windkessel model describing the hydraulic resistance and capacitance in the pulmonary artery and aorta in order to decrease the implementation complexity. This unfortunately also limits the realism in the simulation of late ejection and early filling phases. Our approach differs from [6], where the adjoint method is considered in the continuous setting and then discretized which may add inconsistent discretization errors. The total computation times for one gradient estimation (with forward and backward simulations) is around 45 min on a regular PC, thus leading to computation times of 4 to 6 hours for the mechanical personalization.

B. Calibration Phase

As any gradient-based optimization, our optimization approach is sensitive to initial values. Therefore, we perform a calibration phase of the contractilities based on the ejection fraction. More precisely, kinematics personalization with a standard value of contractility (typically $\sigma_0 = 6 \cdot 10^4 Pa$) is first performed. This leads to a reasonable approximation of the cardiac motion from which the ejection fraction of both ventricles can be estimated. Then several simulations of the electromechanical model are performed (without image forces) with varying values of contractilities in both ventricles until an ejection fraction close to the estimated ones is obtained. We then restart the kinematics personalization with this calibrated set of parameters.

IV. EVALUATION ON SYNTHETIC IMAGES

We evaluate the performance of the joint kinematics and mechanics personalization method on synthetic data. Instead of adding noise to a known simulation, we designed a more comprehensive approach by generating synthetic image sequences using known motion and mechanical parameters. In this case, we considered the electrophysiology and cine MRI dataset from a patient with heart failure. A scar region was detected from late-enhancement MRI and a tetrahedral mesh including the scar region was created (see Fig. 2 (Middle)). We also used patient-specific endocardial activation map measured with the Ensite balloon (St Jude Medical), which was extrapolated to the myocardial volume using an electrophysiological model. The electromechanical model is then run with a fixed set of contractilities in the LV, RV and scar region. We then use the obtained motion field to generate a synthetic MRI sequence from the end-diastolic image.

We apply the calibration stage for both right and left ventricles to obtain a proper initial value of the contractilities (see Fig. 3 (Left)), to find that $10^5 Pa$ is a good initial value. After kinematics personalization we obtain a mesh

which serves as a reference for the mechanics personalization. After 7 iterations, the optimization stops and converges toward contractility values very close from their reference values, with an overestimation of the lowest contractility. On this synthetic sequence, we achieve a good motion recovery, with an average distance error of 0.15 mm between the personalized model and the motion tracking model and an average distance error of 0.14 mm (see Fig. 2 (Right)) with respect to the ground truth (used to simulate images).

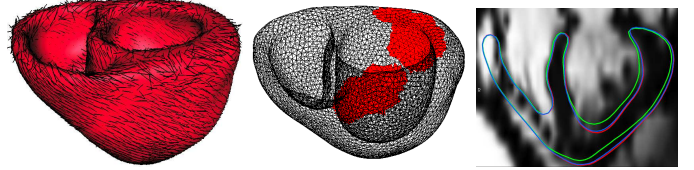


Fig. 2. (Left) Mesh and fiber orientation used for cardiac simulation; (Middle) Scar regions; (Right) Cardiac meshes on long axis image slice; *green*: with initial parameters; *blue*: after mechanics personalization; *red*: ground truth.

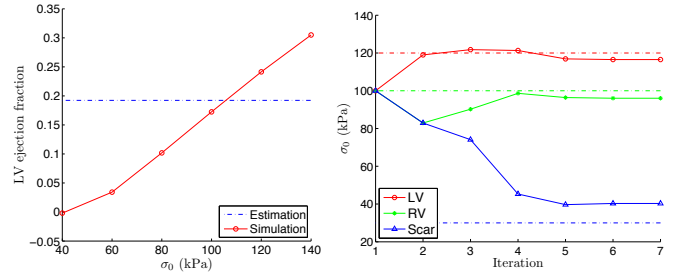


Fig. 3. (Left) Calibration curve of contractility for the left ventricle; (Right) Estimation of 3 regional contractilities.

V. EVALUATION ON CLINICAL DATA

This method was evaluated on the same data as the one used for the synthetic case, but with the actual cine MR image sequence. We estimated the *apparent* contractility parameters σ_0 for each of the three regions using the kinematics and mechanics personalization method. The calibration phase leads to an initial value of $10^5 Pa$ for both ventricles. A good convergence of the 3 parameters is reached with a lower contractility parameter in the scar region as expected (see Fig. 4). The RV contractility is greater than the LV one which may be explained by a greater ejection fraction measured in the RV than in the LV. The optimization decreases the mean distance error with respect to tracked motion (distance between ${}^iY_S^n$ and ${}^iY_E^n$) over the whole cardiac cycle from 2.1 mm to 1.6 mm (see Fig. 5). The average error is comparable to the in-plane image voxel size (1.56 mm^2) but the maximum distance error was 9.7 mm which is significant. The region of largest errors is the base which may imply that the boundary conditions at the base should be improved. However, this is also the region with the largest longitudinal motion and thus with high uncertainty in motion tracking also caused by the large slice thickness (10 mm in such clinical routine sequences). The end diastole is the time at which the average distance error is maximum (2.32 mm). A quantitative comparison of motion with tagged

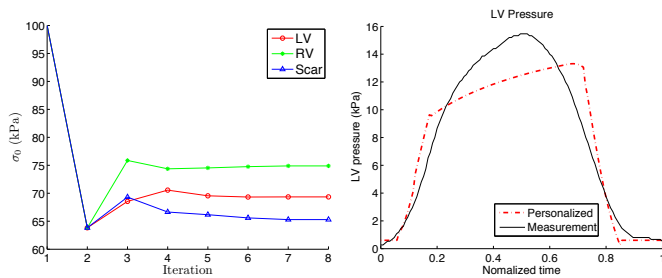


Fig. 4. (Left) Estimation of the contractility parameters for 3 regions of the myocardium; (Right) Estimated and measured pressure curve.

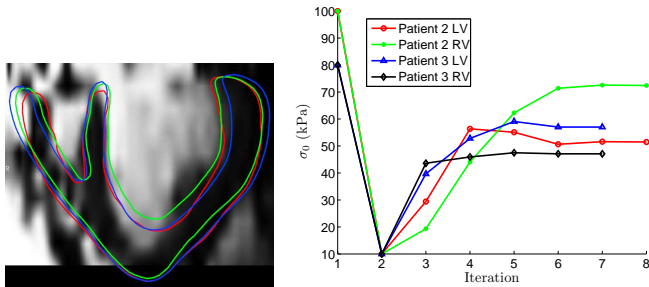


Fig. 5. (Left) Cardiac meshes overlaid on image slice; *green*: with initial contractility parameters; *blue*: after mechanics personalization; *red*: target mesh (after kinematics personalization); movies are available as supplementary material; (Right) Contractility estimation for patients 2 and 3.

MRI in short axis slices for this patient appears to indicate an excellent agreement for the radial motion (maximum errors of 1.2mm) but a decreased accuracy (average errors of 2.5mm) for circumferential motion probably due to the aperture problem. In order to evaluate the realism of the personalized model, we also compared the simulated pressure with the personalized model to the pressure which was invasively measured on that patient during the study. We obtained a fairly good match of this pressure during the contraction phase (see Fig. 4). The maximum value of the rise of pressure $(dP/dt)_{max}$ was decreased from 148 kPa/s to 103 kPa/s after personalization to be compared with a measured $(dP/dt)_{max}$ of 78 kPa/s. The personalization approach was also applied to two additional datasets (using also electrical mappings and cine-MRI) of patients suffering from dilated cardiomyopathy. The estimated contractilities for the RV and LV are rather low (see Fig. 5 (Right)), especially for patient 3. The adjoint method leads to a decrease of the average distance error to 2.33 mm for patient 2 and 2.19 mm for patient 3 (see Fig. 6) for images with respective isotropic voxel size of 1.44 mm and 1.52 mm. One limitation of this work is that it is restricted to the estimation of a limited number of contractility parameters defined on prescribed regions. One could iteratively refine the number of regions where parameters are estimated in a coarse to fine manner like in [8].

VI. CONCLUSION

We presented a new method for the automated mechanical personalization of cardiac models and applied it to several clinical cases including electrophysiology and cine MRI data. Those results are encouraging and their analysis can help

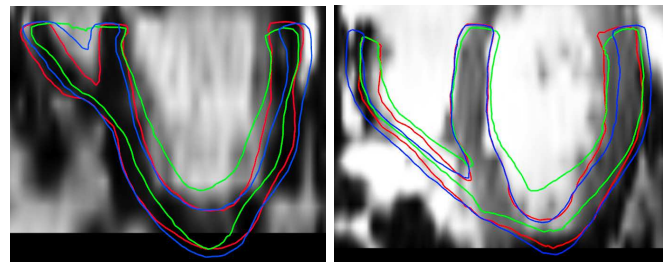


Fig. 6. Overlay of the cardiac mesh after kinematics personalization for patient 2 (Left) and patient 3 (Right) with the same convention as Fig 5; movies are available as supplementary material.

improving the model and the parameter set to be optimized. Those personalized models may serve to plan various therapies (e.g. Cardiac Resynchronization Therapy) by predicting the cardiac function after testing several therapeutic strategies *in silico*.

REFERENCES

- [1] M. Sermesant, F. Billet, R. Chabiniok, T. Mansi, P. Chinchapatnam, P. Moireau, J. Peyrat, K. Rhode, M. Ginks, P. Lambiase, S. Arridge, H. Delingette, M. Sorine, C. Aldo Rinaldi, D. Chapelle, R. Razavi, and N. Ayache, "Personalised electromechanical model of the heart for the prediction of the acute effects of cardiac resynchronisation therapy," in *International Conference on Functional Imaging and Modeling of the Heart*, 2009, pp. 239–248.
- [2] P. Moireau and D. Chapelle, "Reduced-order Unscented Kalman Filtering with application to parameter identification in large-dimensional systems," *COCV*, 2010, published online, doi:10.1051/cocv/2010006.
- [3] J. Xi, P. Lamata, J. Lee, P. Moireau, D. Chapelle, and N. Smith, "Myocardial transversely isotropic material parameter estimation from in-silico measurements based on reduced-order unscented kalman filter," *J. of the Mech. Behavior of Biomedical Materials*, vol. In Press, 2011.
- [4] V. Y. Wang, H. I. Lam, D. B. Ennis, B. R. Cowan, A. A. Young, and M. P. Nash, "Modelling passive diastolic mechanics with quantitative MRI of cardiac structure and function," *Medical Image Analysis*, vol. 13, no. 5, pp. 773–784, 2009.
- [5] H. Liu and P. Shi, "Maximum a posteriori strategy for the simultaneous motion and material property estimation of the heart," *IEEE Trans. on Biomedical Engineering*, vol. 56, no. 2, pp. 378–389, Feb. 2009.
- [6] H. Sundar, C. Davatzikos, and G. Biros, "Biomechanically-constrained 4D estimation of myocardial motion," in *Medical Image Computing and Computer-Assisted Intervention MICCAI 2009*, ser. LNCS, vol. 5762. Springer, 2009, pp. 257–265.
- [7] K. Rhode, M. Sermesant, D. Brogan, S. Hegde, J. Hipwell, P. Lambiase, E. Rosenthal, C. Bucknall, S. Qureshi, J. Gill, R. Razavi, and D. Hill, "A system for real-time XMR guided cardiovascular intervention," *IEEE Transactions on Medical Imaging*, vol. 24, no. 11, pp. 1428–1440, 2005.
- [8] J. Relan, P. Chinchapatnam, M. Sermesant, K. Rhode, M. Ginks, H. Delingette, C. A. Rinaldi, R. Razavi, and N. Ayache, "Coupled personalisation of cardiac electrophysiology models for prediction of ischemic ventricular tachycardia," *Journal of the Royal Society Interface Focus*, 2011, in press.
- [9] F. Billet, M. Sermesant, H. Delingette, and N. Ayache, "Cardiac motion recovery and boundary conditions estimation by coupling an electromechanical model and cine-MRI data," in *Proceedings of FIMH'09*, ser. LNCS, vol. 5528, 3-5 June 2009, pp. 376–385.
- [10] M. Sermesant, H. Delingette, and N. Ayache, "An electromechanical model of the heart for image analysis and simulation," *IEEE Transactions on Medical Imaging*, vol. 25, no. 5, pp. 612–625, 2006.
- [11] K. C. L. Wong, F. Billet, T. Mansi, R. Chabiniok, M. Sermesant, H. Delingette, and N. Ayache, "Cardiac motion estimation using a proactive deformable model: evaluation and sensitivity analysis," in *MICCAI Workshop STACOM*, ser. LNCS, vol. 6364, 2010, pp. 154–163.
- [12] M. Sermesant, P. Moireau, O. Camara, J. Sainte-Marie, R. Andriantsimivavona, R. Cimrman, D. L. Hill, D. Chapelle, and R. Razavi, "Cardiac Function Estimation from MRI Using a Heart Model and Data Assimilation: Advances and Difficulties," *Medical Image Analysis*, vol. 10, no. 4, pp. 642–656, 2006.